한국표면공학회지
*J. Korean Inst. Surf. Eng*
Vol.54, No.2, 2021.
https://doi.org/10.5695/JKISE.2021.54.2.43

ISSN 1225-8024(Print)
ISSN 2288-8403(Online)

〈연구논문〉

# 대기 및 Ar-0.2%$SO_2$가스에서 Inconel 740 합금의 고온부식 연구

이동복[1], 김민정[2*]

[1]성균관대학교 신소재공학과
[2]한국폴리텍대학 신소재응용과

# Study of High Temperature of Inconel 740 Alloy in Air and Ar-0.2%$SO_2$ Gas

Dong Bok Lee[1], Min Jung Kim[2*]

[1]School of Advanced Materials Science and Engineering, Sungkyunkwan University, Suwon 16419, Korea
[2]Advanced material application department, Korea Polytechnic College, 478 Munemiro, Bupyeong-gu, Incheo 21417, Korea

(Received 24 December, 2020 ; revised 25 January, 2021 ; accepted 03 March, 2021)

**Abstract**

The Ni-based superalloy, Inconel 740, was corroded between 800 and 1100°C for up to 100 hr in air and Ar-0.2%$SO_2$ gas in order to study its corrosion behavior in air and sulfur/oxygen environment. It displayed relatively good corrosion resistance in both environment, because its corrosion was primarily dominated by not sulfidation but oxidation especially in Ar-0.2%$SO_2$ gas. Such was attributed to the thermodynamic stability of oxides of alloying elements when compared to corresponding sulfides. The scales consisted primarily of $Cr_2O_3$, together with some $NiAl_2O_4$, $MnCr_2O_4$, $NiCrMnO_4$, and rutile-$TiO_2$. Sulfur from $SO_2$ gas made scales prone to spallation, and thicker. It also widened the internal corrosion zone when compared to air. The corrosion resistance of IN740 was mainly indebted to the formation of protective $Cr_2O_3$-rich oxides, and suppression of the sulfide formation.

*Keywords : Alloys, casting, oxidation, $SO_2$-corrosion, Inconel 740*

## 1. INTRODUCTION

Nickel-based superalloys are widely used as high-temperature structural components because of their superior mechanical strength and resistance to creep, corrosion, and oxidation. Efforts to improve their properties led to the development of Ni-Cr-Co-base Inconel 740 (IN740), which is cast, polycrystalline, and precipitation-hardenable because of $\gamma'$-$Ni_3$(Al,Ti,Nb) precipitates that are dispersed in the *fcc* austenitic ($\gamma$) matrix. Since the corrosion resistance is prerequisite for practical applications, the high-temperature corrosion behavior of IN740 was studied in corrosive

*Corresponding Author: Min Jung Kim
Advanced material application department,
Korea Polytechnic College
Tel.: +82-32-510-2372; fax: +82-32-519-6169
E-mail: mjkim1219@kopo.ac.kr

environments such as air with and without $Na_2SO_4$ deposit [1,2], coal ash hot corrosion [3], and ultra-supercritical boilers [4]. The current research aims to study the corrosion behavior of IN740 at 800-1100 °C in air and $SO_2$-containing gas. Sulfur-containing oxygen environments are encountered in high-temperature gas turbines, heat exchangers, petrochemical units, oil refineries, incinerators, glass vitrification, and coal gasification systems. Sulfidation owing to sulfur in $SO_2$ is more problematic than oxidation, because metal sulfides are less adherent, melt at lower temperatures, and grow fast due to their nonstoichiometry than comparable oxides [5-7]. Generally, $Al_2O_3$ and $Cr_2O_3$ protect superalloys from the corrosive environments. However, the high-temperature corrosion behavior of IN740 in oxygen and oxygen/sulfur environments was not adequately reported. In this study the types and morphologies of the scales formed, the oxidation mechanism, and the oxidation resistance were characterized.

## 2. EXPERIMENTAL PROCEDURES

Cast Inconel 740 (50Ni-25Cr-20Co-2Nb-1.8Ti-0.9Al-0.7Fe-0.5Mo-0.5Si-0.3Mn-0.03C in wt.%) were cut into small coupons with dimensions of 10 x 10 x 2 $mm^3$, polished with a 1000 grit SiC paper, ultrasonically cleaned in acetone and methanol, and oxidized at 800, 900, and 1000 °C for 5-100 h in atmospheric air and Ar (99.999% purity)-0.2% $SO_2$ (99.9% purity) gas using a thermogravimetric analyser. The formed scales were investigated using a scanning electron microscope equipped with an energy-dispersive spectroscope (SEM-EDS; S-3000H, Hitachi, Japan), an electron probe microanalyzer (EPMA; JXA-8900R, Jeol, Japan), an X-ray diffractometer (XRD; M18XHF-SRA, Mac Science, Japan) with Cu-K$\alpha$ radiation at 40 kV and 150 mA in a $\theta/2\theta$ configuration and a transmission electron microscope (TEM; JEM-2100F, Jeol, Japan operated at 200 keV) equipped with EDS with a 5-nm spot size. The TEM sample was prepared using a focused ion beam milling system after carbon coating.

## 3. RESULTS AND DISCUSSION

Figure 1 shows corrosion kinetics of IN740 in air and Ar/0.2% $SO_2$ gas. Weight gains are plotted as a function of corrosion time in Fig. 1(a), whereas the parabolic plots are given in Fig. 1(b). In Fig. 1(a), small weight gains were recorded in both air and 0.2% $SO_2$, displaying relatively good corrosion resistance of IN740. Corrosion rates increased with increasing the temperature from 800 °C to 1100 °C, and changing the environment from air to 0.2% $SO_2$ gas. Sulfur in $SO_2$ clearly increased the corrosion rate. Sulfur is known to impede the chromia formation [8], decrease the plasticity of the scale by dissolving in the scale, and deteriorate scale adherence by segregating at the scale/alloy interface [9].

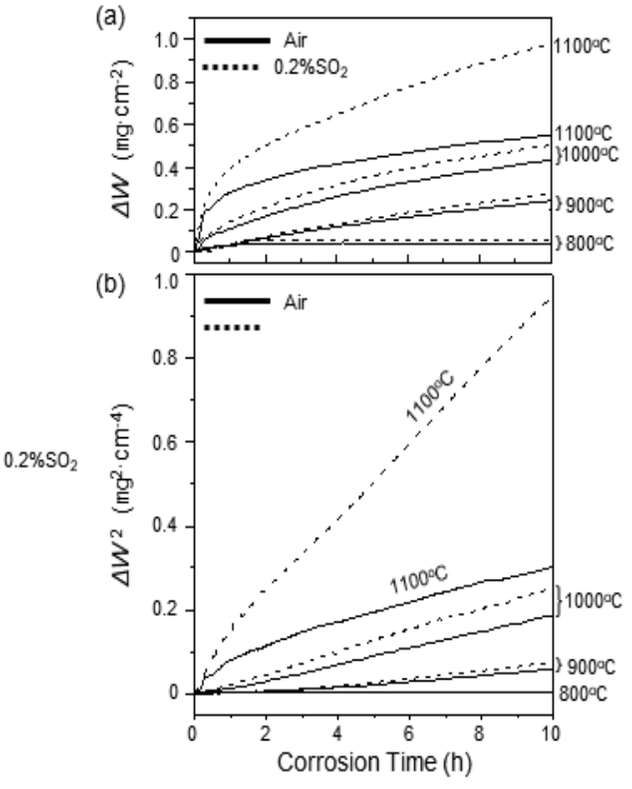


**Fig. 1.** Corrosion kinetics of IN740 in air and Ar/0.2% $SO_2$ gas at 800-1100 °C for 10 h. (a) weight gain versus time curves, (b) parabolic plot of (a).

$$2Cr + 3/2O_2 \rightarrow Cr_2O_3$$

$$2Cr + 3/2S_2 \rightarrow Cr_2S_3$$

Figure 1(b) indicates that IN740 corroded almost parabolically in air and 0.2% $SO_2$, after the initial, transient corrosion period, suggesting that the corrosion was diffusion-controlled.

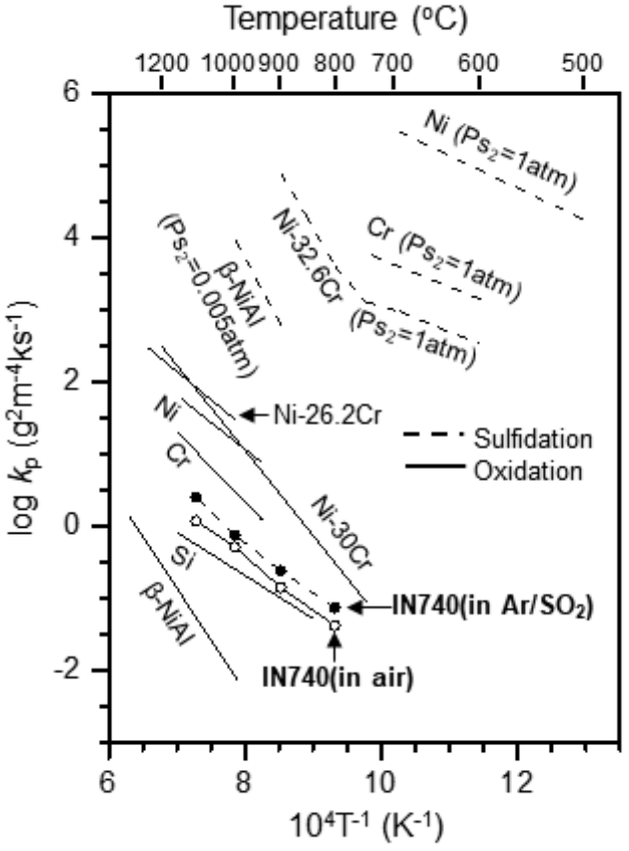


**Fig. 2.** Temperature dependence of parabolic rate constants of IN740 in air and Ar/0.2% $SO_2$ gas at 800-1100 °C. Values of $k_p$ for oxidation of Ni, Cr, Si, β-NiAl [10], Ni-26.2 wt%Cr alloy [11], and Ni-30 wt.%Cr alloy [12] as well as sulfidation of Ni [12], Cr [13], β-NiAl [14], and Ni-32.6 wt.%Cr alloy [15] are superimposed for comparison.

Using the parabolic corrosion equation, $\Delta W^2 = k_p \cdot t$, where $\Delta W$ is the weight gain per unit area, $t$ is the corrosion time, and $k_p$ is the parabolic rate constant, $k_p$ values were calculated, excluding the initial, transient corrosion period. Values $k_p$ of IN740 are displayed in the Arrehnius plot shown in Fig. 2 for the corrosion temperatures of 800, 900, 1000, and 1100 °C in air and 0.2% $SO_2$ gas. For comparison purpose, oxidation and sulfidation rates of essential elements in IN740 as well as some Ni-based alloys are superimposed. The oxidation of Ni, Cr, Si, β-NiAl [10], Ni-26.2Cr alloy [11], and Ni-30Cr alloy [12] led to the formation of oxides of NiO, $Cr_2O_3$, $SiO_2$, α-$Al_2O_3$, and $Cr_2O_3$, respectively, whilst the sulfidation of Ni [12], Cr [13], β-NiAl [14], and Ni-32.6Cr alloy [15] led to the formation of sulfides of NiS, $Cr_2S_3$, $NiAl_2S_4$, and (NiS+$Cr_2S_3$), respectively. In Fig. 2, sulfidation rates are much faster than corresponding oxidation rates due primarily to higher concentration and/or mobility of point defects in the nonstoichiometric sulfides [12]. In air and 0.2% $SO_2$ gas, IN740 corroded a little slower than chromia-forming kinetics [10-12], however, faster than silica- and α-alumina- forming kinetics [10]. Nevertheless, IN740 displayed relatively good corrosion resistance in air and 0.2% $SO_2$ gas, because $Cr_2O_3$-rich scales formed without forming any discernable sulfides, as shown in Fig. 3.

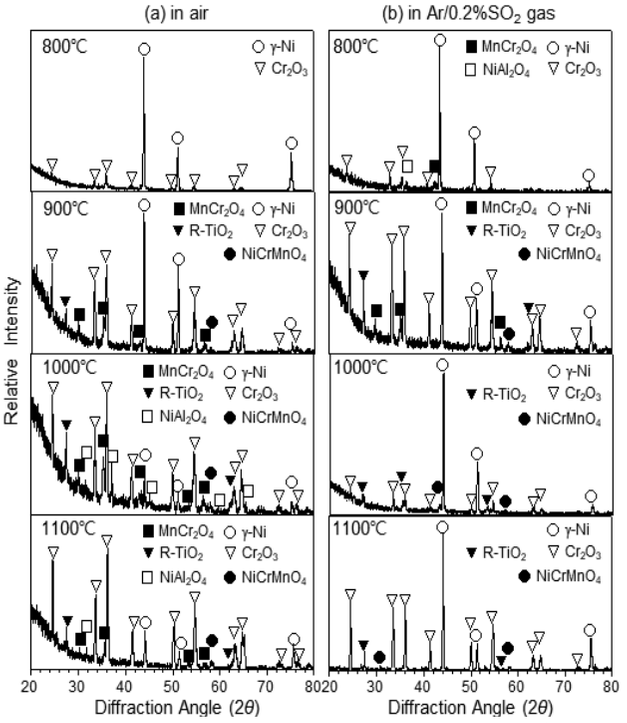


**Fig. 3.** XRD patterns of the scales formed on IN740 after corrosion for 50 h at 800, 900, 1000, and 1100 °C in (a) air, and (b) Ar/0.2% $SO_2$ gas.

Figure 3 shows XRD patterns of IN740 after corrosion for 50 h at 800-1100 °C in air and 0.2% $SO_2$ gas. Phases identified in Fig. 3 are listed in Table 1. The γ-Ni matrix pattern was always identified, because the formed $Cr_2O_3$-rich scales were either thin owing to small extent of corrosion, or partial

scale spallation that occurred during corrosion and the subsequent handling stage. Poor adherence of scales was inevitably noticed in air and 0.2% $SO_2$ gas. Chromia always formed from the early corrosion stage. It protected IN740 as the major corrosion product. Additionally, some amounts of $NiAl_2O_4$, rutile-$TiO_2$, $MnCr_2O_4$, and a bit of $NiCrMnO_4$ formed as corrosion proceeded in air and 0.2% $SO_2$ gas.

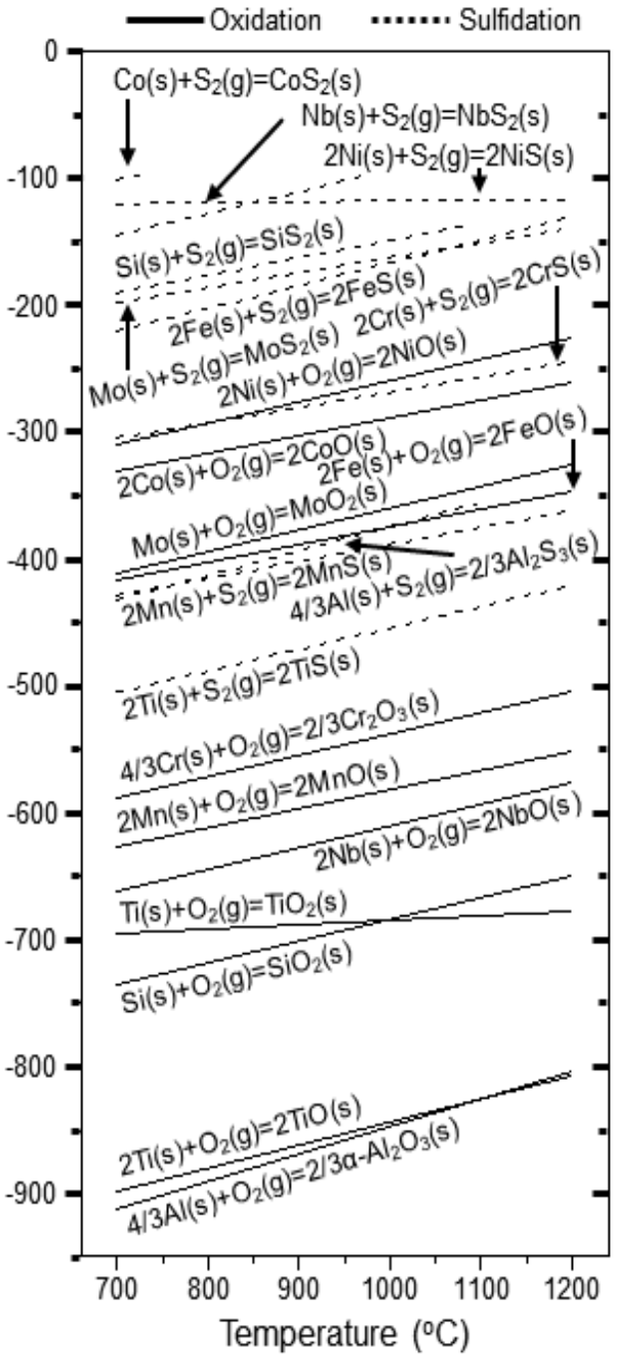


**Fig. 4.** Ellingham diagram for oxidation and sulfidation of Ni, Cr, Co, Nb, Ti, Al, Fe, Mo, Si, and Mn[16].

Figure 4 shows the Ellingham diagram for the oxidation and sulfidation of essential elements in IN740 [16]. The sulfide stability increased in the order of $CoS_2$, $NbS_2$ or NiS, $SiS_2$, $MoS_2$ or FeS, CrS, $Al_2S_3$ or MnS, and TiS, whilst the oxide stability increased in the order of NiO, CoO, $MoO_2$, FeO, $Cr_2O_3$, MnO, NbO, rutile-$TiO_2$ or $SiO_2$, and TiO or $\alpha$-$Al_2O_3$. The absence of sulfides in the scales that formed in 0.2% $SO_2$ gas, as listed in Table 1, was due to the following reasons; (1) all the oxides were thermodynamically more stable than the corresponding sulfides. (2) sulfides might be dissolved in oxides that were listed in Table 1, or their amount might be too small to detect using XRD. During corrosion in air and 0.2% $SO_2$ gas, the active element, Al, oxidized to the $NiAl_2O_4$ spinel (Table 1). $\alpha$-$Al_2O_3$ was absent in Table 1, probably due to its dissolution in isostructural $Cr_2O_3$[17]. Both oxides have the corundum structure. Another active element, Ti, oxidized rapidly to rutile-$TiO_2$ through the initial, transient TiO[17] (Table 1). $TiO_2$ is not protective, because it grows much faster than $Al_2O_3$ owing to its high lattice defect concentration. The relatively active element, Mn, oxidized to $MnCr_2O_4$ or $NiCrMnO_4$ spinels (Table 1). Another relatively active element, Cr, oxidized to $Cr_2O_3$ with a high degree of stoichiometry, and some of which further oxidized to $MnCr_2O_4$ and $NiCrMnO_4$ (Table 1). Since Cr was the second most rich element next to the noble Ni in IN740, $Cr_2O_3$ became the major corrosion product. The base metal, Ni, oxidized to NiO, $NiAl_2O_4$, and $Ni_2Cr_2O_4$ (Table 1). However, no oxides of Co, Nb, Fe, Mo, and Si were detected owing to their thermodynamic nobility[9-10], small amount in formed scales, or dissolution in oxides that were listed in Table 1. The corrosion resistance of IN740 was mainly indebted to the formation of protective $Cr_2O_3$-rich oxides, and suppression of the sulfide formation.

**Table 1.** Phases identified in Fig. 3

| | in air | in Ar/0.2% $SO_2$ |
|---|---|---|
| 800°C | $\gamma$-Ni(vs), $Cr_2O_3$(m) | $\gamma$-Ni(vs), $Cr_2O_3$(w), $MnCr_2O_4$(vw), $NiAl_2O_4$(vw) |
| 900°C | $\gamma$-Ni(vs), $Cr_2O_3$(s), R-$TiO_2$(w), $MnCr_2O_4$(w), $NiCrMnO_4$(vw) | $\gamma$-Ni(vs), $Cr_2O_3$(s), R-$TiO_2$(vw), $MnCr_2O_4$(w), $NiCrMnO_4$(vw) |
| 1000°C | $\gamma$-Ni(w), $Cr_2O_3$(vs), $NiAl_2O_4$(m), R-$TiO_2$(m), $MnCr_2O_4$(m), $NiCrMnO_4$(w) | $\gamma$-Ni(vs), $Cr_2O_3$(w), R-$TiO_2$(w), $NiCrMnO_4$(vw) |
| 1100°C | $\gamma$-Ni(m), $Cr_2O_3$(vs), $NiAl_2O_4$(m), R-$TiO_2$(m), $MnCr_2O_4$(w), $NiCrMnO_4$(w) | $\gamma$-Ni(vs), $Cr_2O_3$(s), R-$TiO_2$(m), $NiCrMnO_4$(vw) |

Remark; (vs)= very strong, (s)= strong, (m)= medium, (w)= weak, and (vw)= very

Figure 5 shows SEM images of IN740 after oxidation at 800 °C for 50 h in air. The surface was covered with fine oxide grains, which aligned along grinding grooves that formed during sample preparation (Fig. 5(a)). Fine oxide grains indicated that corrosion occurred to a small extent. Internal oxides formed down to ~ 2 $\mu$m in depth underneath ~1.5 $\mu$m-thick, partially broken oxide scale (Fig. 5(b)).

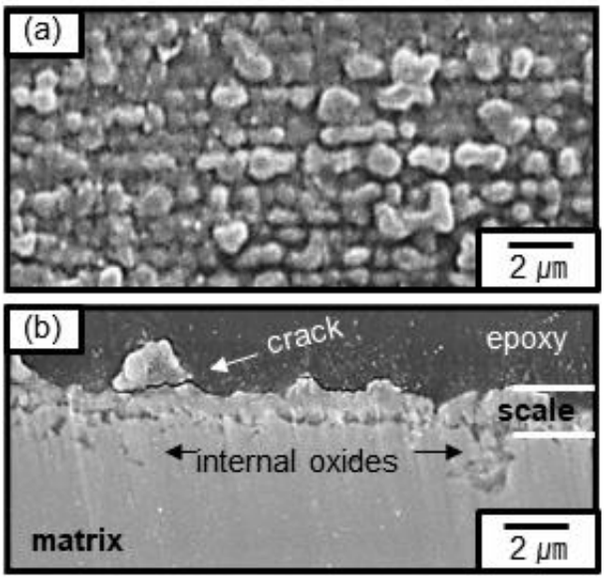


**Fig. 5.** SEM images of IN740 after oxidation at 800 °C for 50 h in air. (a) top view, (b) cross-section view.

Figure 6 shows SEM/EDS results of IN740 after oxidation at 800 °C for 100 h in air. Since IN740 had relatively good oxidation resistance, the $Cr_2O_3$-rich scale was still thin (Fig. 6(a)). It surrounded the less oxidation-resistant TiC inclusions scattered in the matrix. TiC oxidized to rutile-$TiO_2$ [18,19]. $TiO_2$ is known to grow by both the outward diffusion of $Ti^{4+}$ ions and the inward diffusion of $O^{2-}$ ions [20], which could be recognizable in Fig. 6(b)-(e). The formation of numerous internal oxide precipitates resulted from the inward diffusion of oxygen across the $Cr_2O_3$-rich scale and, probably, along TiC/matrix phase boundaries.

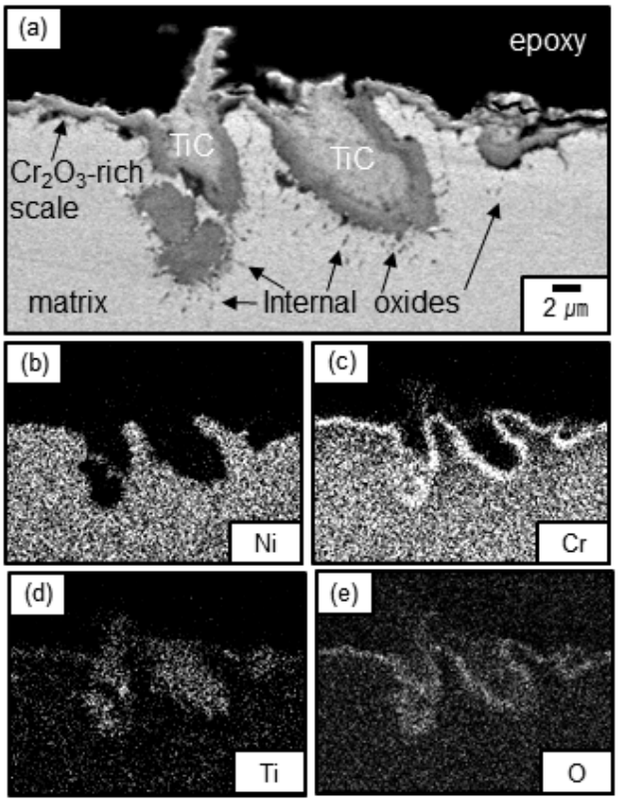


**Fig. 6.** SEM/EDS results of IN740 after oxidation at 800 °C for 100 h in air. (a) cross-sectional back-scattered electron (BSE) image, (b) mapping of Ni, (c) mapping of Cr, (d) mapping of Ti, (e) mapping of oxygen.

Figure 7 shows EPMA results of IN740 after oxidation at 900 °C for 50 h in air. The scale grew to ~11 $\mu$m in thickness. Internal oxides formed to the depth of ~15 $\mu$m (Fig. 7(a)). A blocky, unoxidized TiC carbide is seen in the matrix [19]. Ni did not incorporate much in the oxide scale owing to its thermodynamic nobility, despite of its abundance in the alloy (Fig. 7(b)). $TiO_2$, $MnCr_2O_4$, $NiCrMnO_4$, and

$NiAl_2O_4$, which were listed in Table 1, were present in the continuous $Cr_2O_3$ layer (Fig. 7(b)). The preferential oxidation of thermodynamically active elements such as Ti, Mn, Cr, and Al was similarly reported during oxidation of Ni-base Inconel alloys [21]. Nb was hardly incorporated in the oxide scale due mainly to its small amount in the alloy. Most internal oxides were rich in Al, Ti, and Co (Fig. 7(e)(f)). Relatively noble elements such as Co and Ni tended to be expelled from the growing oxide scale, leading to their segregation around the scale/alloy interface. Here, the minor alloying element, Si, segregated owing to its low activity. Generally, the amount and distribution of metallic elements in the oxide scale depended on the thermodynamic activity and diffusivity of each element and the oxygen potential in the scale[10].

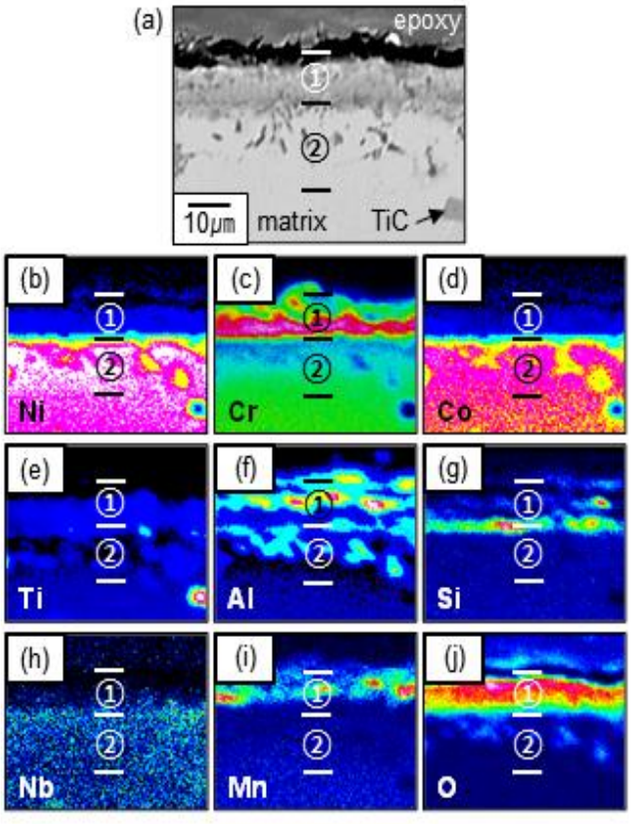


**Fig. 7.** EPMA results of IN740 after oxidation at 900 °C for 50 h in air. (a) cross-sectional BSE image, (b) map of Ni, (c) map of Cr, (d) map of Co, (e) map of Ti, (f) map of Al, (g) map of Si, (h) map of Nb, (i) map of Mn, (j) map of O. ①=oxide scale, ②=internal oxidation zone.

A similar oxide scale as shown in Fig. 7 was displayed in Fig. 8, indicating that the increment of oxidation temperature from 900 °C to 1000 °C did not change the overall scale structure. Grain boundaries oxidized preferentially, and oxides spalled locally (Fig. 8(a)), which was usual in this study. The scale was about 12 μm-thick, and internal oxidation occurred to ~20 μm in depth (Fig. 8(b)-(j)). The oxide scale consisted primarily of $Cr_2O_3$, with less amounts of $TiO_2$, $MnCr_2O_4$, $NiCrMnO_4$, and $NiAl_2O_4$ (Table 1). Particularly, $Cr_2O_3$ and $MnCr_2O_4$ existed as continuous layers (Fig. 8(c)-(k)). As did in Fig. 7(b), Ni and Co did not incorporate in the oxide scale much due mainly to their thermodynamic nobility, despite their abundance (Fig. 8(c)(f)). Internal oxides were rich in Al and Ti (Fig. 8(h)(i)), because these elements had high oxygen affinity (Fig. 4). They were incorporated with some Ni, Cr and Co, which were the major elements in the alloy (Fig. 8(c)-(f)). Minor alloying elements such as Si and Nb were mostly segregated around the scale/alloy interface (Fig. 8(j)(k)), as did in Fig. 7(b)-(j).

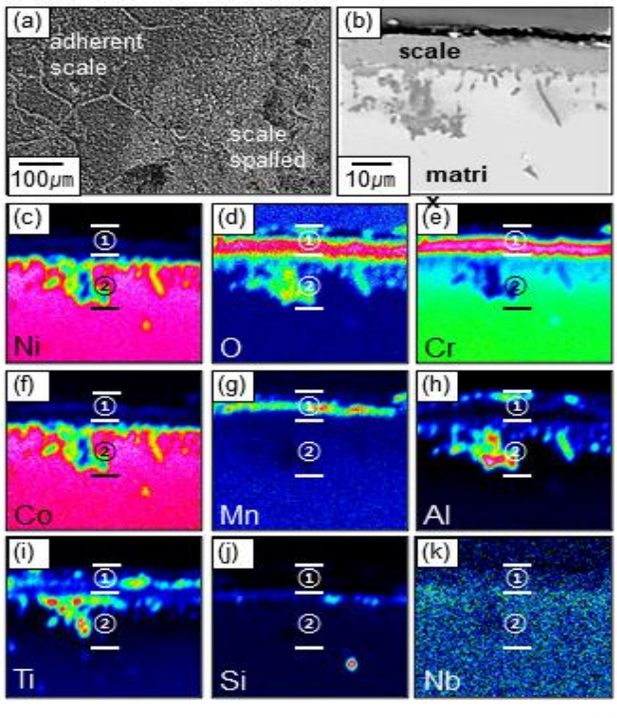


**Fig. 8.** IN740 after oxidation at 1000 °C for 50 h in air. (a) SEM top view, (b) EPMA cross-sectional BSE image, (c) map of Ni, (d) map of O, (e) map of Cr, (f) map of Co, (g) map of Mn, (h) map of Al, (i) map of Ti, (j) map of Si, (k) map of Nb. ①=oxide scale, ②=internal oxidation zone.

When corroded in air or Ar-0.2% $SO_2$ gas, the same kind of oxides formed on IN740 as listed in Table 1. Which indicated that sulfur from $SO_2$ gas was dissolved in the oxide scale or the amount of sulfides that formed owing to $SO_2$ gas. It was too small to detect from the XRD analysis. During corrosion at 800-1100 °C for 10-100 h, the scales and internal oxidation zones that formed in 0.2% $SO_2$ gas were generally thicker compared to those formed in air, as listed in Table 2. The main difference was that scales spalled and broke more in $SO_2$ gas than in air, because the surface active sulfur deteriorated the scale adherence by segregating on the surface of voids and cracks at the alloy/oxide interface [8]. Such scale failure facilitated the corrosion in $SO_2$ gas.

**Table 2.** Thickness of the scales and internal oxidation zones that formed during corrosion at 800-1100 °C for 10-100 h in air and Ar/$SO_2$ gas.

| | at 800°C | 10 h | 50 h | 75 h | 100 h |
|---|---|---|---|---|---|
| in air | scale | 1.85 | 2.56 | 2.74 | 3.97 |
| | IOZ | 2.48 | 2.51 | 2.67 | 4.01 |
| in Ar/$SO_2$ | scale | - | 5.52 | - | 6.67 |
| | IOZ | - | 8.76 | - | 7.14 |
| | **at 900°C** | **10 h** | **50 h** | **75 h** | **100 h** |
| in air | scale | 3.50 | 6.04 | 11.75 | 6.67 |
| | IOZ | 10.63 | 9.06 | 12.13 | 10.00 |
| in Ar/$SO_2$ | scale | - | 6.84 | - | 13.70 |
| | IOZ | - | 10.00 | - | 10.37 |
| | **at 1000°C** | **10 h** | **50 h** | **75 h** | **100 h** |
| in air | scale | 4.50 | 10.43 | 11.11 | 11.88 |
| | IOZ | 11.00 | 23.74 | 28.33 | 29.95 |
| in Ar/$SO_2$ | scale | - | 11.67 | - | 135.55 |
| | IOZ | - | 29.63 | - | 111.11 |
| | **at 1100°C** | **10 h** | **50 h** | **75 h** | **100 h** |
| in air | scale | 12.96 | 21.85 | - | 10.00 |
| | IOZ | 17.40 | 28.33 | - | 18.75 |
| in Ar/$SO_2$ | scale | 4.75 | 9.26 | - | 14.44 |
| | IOZ | 3.63 | 24.07 | - | 25.93 |

Fig. 9 shows EPMA results of the retained scale that formed on IN740 after corrosion at 1100 °C for 100 h in $SO_2$ gas. The scale spalled off partially and broke easily for the following reasons (Fig. 9(a)); (1) corrosion at a high temperature for a long time in $SO_2$ gas thickened the scale much, (2) large growth stress generated in the scale, (3) large thermal stress developed owing to mismatch in thermal expansion coefficients among oxides and the matrix, (4) voids formed owing to the outwardly diffusing cations to form the scale, and (5) anisotropic volume expansion aroused during scaling. Sulfur dissolved in the $Cr_2O_3$-rich scale and internal corrosion zone (Fig. 9(b)-(d)). Sulfur distributed nonuniformly due to its relatively small solubility in the oxides and alloy [22]. It diffused inwardly deeper than oxygen, because most of oxygen was consumed to form the $Cr_2O_3$-rich scale above. It can diffuse rapidly through the lattice, grain boundaries or dislocation pipes in the oxide, and microcracks[22]. The incompact, heterogeneous, nonuniform scale might possess low plasticity. Such a scale could not be a good diffusion barrier between matrix and reaction gas.

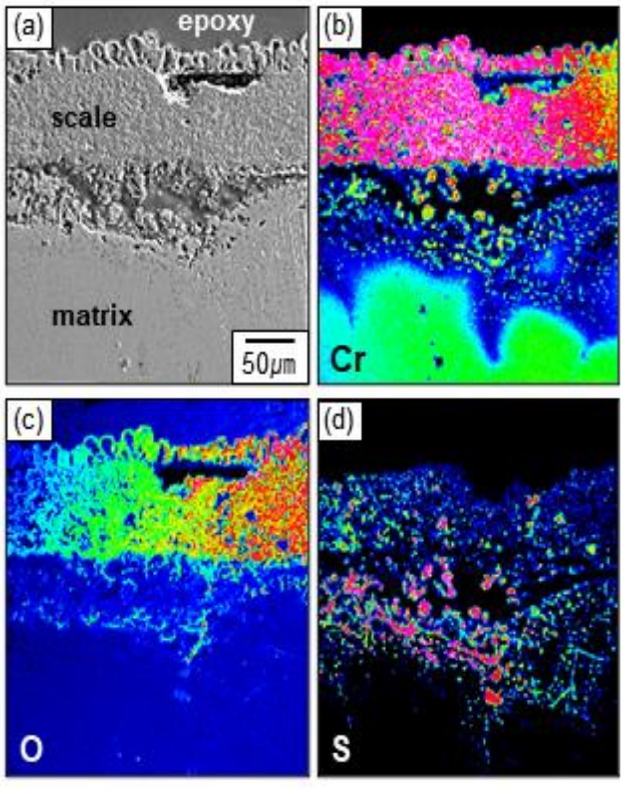


**Fig. 9.** EPMA results of IN740 after corrosion at 1100 °C for 100 h in Ar-0.2% $SO_2$ gas. (a) cross-sectional image, (b) map of Cr, (c) map of O, (d) map of S.

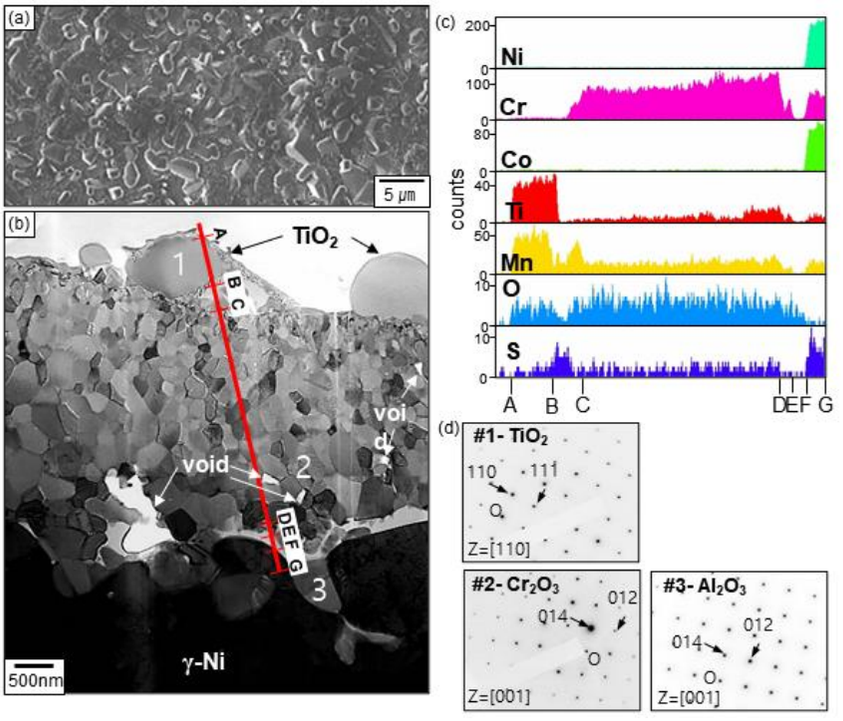


**Fig. 10.** IN 740 after corrosion at 1000 °C for 10 h in Ar-0.2% $SO_2$ gas. (a) SEM top view, (b) cross-sectional TEM image, (c) EDS concentration profiles along the line A-G denoted in (b), (d) selected area electron diffraction (SADP) patterns of the grain #1, 2, and 3 denoted in (b).

Figure 10 shows SEM/TEM/EDS results of IN 740 after corrosion at 1000 °C for 10 h in Ar-0.2% $SO_2$ gas. The surface of the scale was covered with fine, round oxide grains (Fig. 10(a)). The scale was about 3-5 $\mu$m thick in the viewing area (Fig. 10(b)). In Fig. 10(c), the line A-B, B-C, C-D, and D-E correspond to a round $TiO_2$ grain, a fine $MnCr_2O_4$ grain, round, submicrometer-size $Cr_2O_3$ grains, and the $\gamma$-Ni matrix respectively. Complementary data shown in Fig. 10(d) indicate that grain #1, 2, and 3 denoted in Fig. 10(b) were $Cr_2O_3$, $\alpha$-$Al_2O_3$, and rutile-$TiO_2$, respectively. The highly stable $TiO_2$ surface grains were coarser than underlying grains owing to its nonstoichiometry. The formation of $TiO_2$ on the $Cr_2O_3$ layer was similarly observed in Ni-25%Cr-0.25%C alloys that oxidized at 1200 °C in air [23]. Outer $TiO_2$ grains formed by the outward diffusion of $Ti^{4+}$ ions, which depleted Ti underneath (Fig. 10(c)). They had a small amount of dissolved Cr and Mn ions, which also diffused outwardly along grain boundaries of the $Cr_2O_3$ layer [24]. Mn with high oxygen affinity oxidized to the slowly growing $MnCr_2O_4$ spinel at the line B-C. Grains of $MnCr_2O_4$ were as fine as 0.2 $\mu$m. $Cr_2O_3$ grains had 0.3-0.8 at.%Ti, according to the TEM/EDS spot analysis. Their growth was governed by counter diffusion of oxygen and chromium along oxide grain boundaries [25]. Titanium in chromia-forming alloys adversely accelerated the oxidation rate by perturbing the Cr diffusion [23]. The outward diffusion of cations and anisotropic volume expansion during scaling developed microscopic voids especially at the lower part of the scale (Fig. 10(b)). Sulfur was weakly detected around the point B and line D-E. Ni and Co tended to be expelled from the growing scale owing to their nobility, despite their abundance in IN740.

## 4. CONCLUSIONS

Inconel 740 displayed relatively good corrosion resistance at 800~1100 °C for 10-100 h in air and Ar-0.2%$SO_2$ gas. In both atmospheres, it corroded almost parabolically, implying that its corrosion was diffusion-controlled. In both atmospheres, $Cr_2O_3$-rich scales formed with little sulfides, indicating that not sulfidation but oxidation prevailed

in Ar-0.2%$SO_2$ gas. Such preferential oxidation was mainly attributed to thermodynamic stability of oxides when compared to sulfides. Chromia always formed from the early corrosion stage. It protected IN740 as the major corrosion product in both atmospheres. Additionally, some amounts of $NiAl_2O_4$, rutile-$TiO_2$, $MnCr_2O_4$, and a bit of $NiCrMnO_4$ formed as the corrosion proceeded. Sulfur from $SO_2$ gas could form sulfides, which might be dissolved in oxide scales. Otherwise, the amount of sulfides that formed owing to $SO_2$ gas was too small to detect from the XRD analysis. The scale spalled and broke more easily in Ar-0.2%$SO_2$ gas than in air because the surface active sulfur deteriorated the scale adherence. Such scale failure facilitated the corrosion in $SO_2$ gas. Sulfur diffused inwardly deeper than oxygen, because most of oxygen was consumed to form the $Cr_2O_3$-rich scale above. Ingress of sulfur and oxygen led to formation of the internal corrosion zone below the oxide scales in both atmospheres.

## ACKNOWLEDGEMENTS

This research was supported by Basic Science Research Program through the National Research Foundation of Korea (NRF) funded by the Ministry of Education (NRF-2019R1A2C1002641).

## REFERENCES

[1] S. Zhao, X. Xie, G. D. Smith, The oxidation behavior of the new nickel-based superalloy Inconel 740 with and without $Na_2SO_4$ deposit, Surface and Coatings Technology 185 (2004) 178-183.

[2] M. Abbasi, D. I. Kim, J. H. Shim, W. S. Jung, Effects of alloyed aluminum and titanium on the oxidation behavior of Inconel 740 superalloy, Journal of Alloys and Compounds 658 (2016) 210-221.

[3] N. Aung, X. Liu, Effect of temperature on coal ash hot corrosion resistance of Inconel 740 superalloy, Corrosion Science 82 (2014) 227-238.

[4] S. Zhao, X. Xie, G. D. Smith, S. J. Patel, Research and improvement on structure stability and corrosion resistance of nickel-base superalloy Inconel alloy 740, Materials & Design 27 (2006) 1120-1127.

[5] S. Mrowec, K. Przybylski, Transport properties of sulfide scales and sulfidation of metals and alloys, Oxidation of Metals 23 (1985) 107-139.

[6] M. Danielewski, S. Mrowec, A. Stołosa, Sulfidation of iron at high temperatures and diffusion kinetics in ferrous sulfide, Oxidation of Metals 17 (1982) 77-97.

[7] P. Kofstad, High Temperature Materials Corrosion in Coal Gasification Atmospheres, (ed. J. F. Norton), p. 1, Elsevier Applied Science Publishers, UK (1984).

[8] H. J. Grabke, Surface and interface segregation in the oxidation of metals, Surface and Interface Analysis 30 (2000) 112 - 119.

[9] P. Y. Hou, Shreir's Corrosion, 4th ed., (eds R. A. Cottis, M. J. Graham, R. Lindsay, S. B. Lyon, J. A. Richardson, J. D. Scantlebury, and F. H. Stott), p. 195, Elsevier, UK (2010).

[10] N. Birks, G. H. Meier, F. S. Pettit, Introduction to the High-Temperature Oxidation of Metals, 2nd ed., p. 62, Cambridge University Press, UK (2006).

[11] S. Espevik, R. A. Rapp, P. L. Daniel, J. P. Hirth, Oxidation of Ni-Cr-W ternary alloys, Oxidation of Metals 14 (1980) 85-108.

[12] S. Mrowec, The problem of sulfur in high-temperature corrosion, Oxidation of Metals 44 (1995) 177-209.

[13] S. Mrowec and M. Zastawnik, On the defect structure of chromium sulphide, Journal of Physics and Chemistry of Solids 27 (1966) 1027-1030.

[14] E. Godlewska, High temperature corrosion of $\beta$-NiAl intermetallic compound and pseudobinary NiAl-Cr alloys in sulphur-containing atmospheres, Materials and Corrosion 48 (1997) 687-699.

[15] S. Mrowec, T. Werber, M. Zastawnik, The mechanism of high temperature sulphur

corrosion of nickel-chromium alloys, Corrosion Science 6 (1966) 47-68.

[16] I. Barin, Thermochemical Data of Pure Substances, VCH, Germany (1989).

[17] A. Rahmel, P. J. Spencer, Thermodynamic aspects of TiAl and $TiSi_2$ oxidation: the Al-Ti-O and Si-Ti-O phase diagrams, Oxidation of Metals 35 (1991) 53-68.

[18] C. J. Cowen, P. E. Danielson, P. D. Jablonski, Journal of Materials Engineering and Performance 20 (2011) 1078-1083.

[19] Y. Tan, X. You, Q. You, J. Li, S. Shi, P. Li, The Precipitation Behavior and Hot Deformation Characteristics of Electron Beam Smelted Inconel 740 Superalloy, Materials Characterization 114 (2016) 267-276.

[20] S. A. Kekare, P. B. Aswath, Oxidation of TiAl based intermetallics, Journal of Materials Science 32 (1997) 2485-2499.

[21] D. B. Lee, High-temperature oxidation of Ni-based Inconel 713 alloys at 800-1100℃ in air, Journal of the Korean institute of surface engineering 44 (2011) 196.

[22] H. J. Grabke, High Temperature Materials Corrosion in Coal Gasification Atmospheres (ed. J. F. Norton), Elsevier Applied Science Publishers, UK (1984) p. 59.

[23] P. Berthod, F. Allègre, E. Kretz, Influence of Titanium on the High Temperature Oxidation and Chromia Volatilization of Ternary Ni-Cr-C Alloys, Oxidation of Metals 86 (2016) 581-595.

[24] A. C. S. Sabioni, A. M. Huntz, L. C. Borges, F. Jomard, First study of manganese diffusion in Cr2O3 polycrystals and thin films by SIMS, Philosophical Magazine 87 (2007) 1921-1937.

[25] B. Pieraggi, in Shreir's Corrosion, 4th ed., Vol. 1, (eds. R. A. Cottis, M. J. Graham, R. Lindsay, S. B. Lyon, J. A. Richardson, J. D. Scantlebury, and F. H. Stott), pp. 101-152, Elsevier, UK (2010).